SEDIMENTOLOGY the journal of the International Association of Sedimentologists

Sedimentology (2016) doi: 10.1111/sed.12247

Variability in bedform morphology and kinematics with transport stage

JEREMY G. VENDITTI*, C.-Y. MARTIN LIN* and MOSLEM KAZEMI†
**Department of Geography, Simon Fraser University, Burnaby, British Columbia, Canada V5A 1S6 (E-mail: jeremy_venditti@sfu.ca)*
†Brain Corporation, San Diego, CA 92121, USA

Associate Editor – David Mohrig

ABSTRACT

Bedform geometry is widely recognized to be a function of transport stage. Bedform aspect ratio (height/length) increases with transport stage, reaches a maximum, then decreases as bedforms washout to a plane bed. Bedform migration rates are also linked to bedform geometry, in so far as smaller bedforms in coarser sediment tend to migrate faster than larger bedforms in finer sediment. However, how bedform morphology (height, length and shape) and kinematics (translation and deformation) change with transport stage and suspension have not been examined. A series of experiments is presented where initial flow depth and grain size were held constant and the transport stage was varied to produce bedload dominated, mixed-load dominated and suspended-load dominated conditions. The results show that the commonly observed pattern in bedform aspect ratio occurs because bedform height increases then decreases with transport stage, against a continuously increasing bedform length. Bedform size variability increased with transport stage, leading to less uniform bedform fields at higher transport stage. Total translation-related and deformation-related sediment fluxes all increased with transport stage. However, the relative contribution to the total flux changed. At the bedload dominated stage, translation-related and deformation-related flux contributed equally to the total flux. As the transport stage increased, the fraction of the total load contributed by translation increased and the fraction contributed by deformation declined because the bedforms got bigger and moved faster. At the suspended-load dominated transport stage, the deformation flux increased and the translation flux decreased as a fraction of the total load, approaching one and zero, respectively, as bedforms washed out to a plane bed.

Keywords Bedform deformation, bedform translation, bedforms, dunes, sand-bedded rivers, sediment flux.

INTRODUCTION

Bedforms in sand-bedded rivers are the dominant source of flow resistance, and their formation, growth and kinematics control sediment flux; they also leave characteristic signatures of their presence in the sedimentary record that allow for reconstruction of palaeoflows. Cross-stratified units made up of cross-sets preserved between two successive erosional surfaces are one of the most common structures in sedimentary strata (Allen, 1970; Rubin & Hunter, 1982). These cross-sets have characteristic signatures that record bedform size, shape, migration rate and direction (Allen, 1973). Cross-set thickness can be used to estimate bedform height (Paola & Borgman, 1991; Leclair, 2002; Jerolmack & Mohrig, 2005; Ganti et al., 2013) which is frequently

© 2015 The Authors. Sedimentology © 2015 International Association of Sedimentologists

used to estimate formative flow depths in rivers (e.g. Bridge & Tye, 2000). The controls bedforms exert on flow resistance and sediment flux in rivers, and their use in palaeoflow estimation, is critically dependent on current understanding of how bedform dimensions and kinematics respond to flow strength.

It is widely recognized that bedform dimensions are a function of transport stage (Yalin, 1972; Yalin & Karahan, 1979a, Allen, 1982; van Rijn, 1984; Venditti *et al.*, 2005; Venditti, 2013; Lin & Venditti, 2013) and bedform dimensions are thought to influence migration rates (Allen, 1973; Raudkivi & Witte, 1990; Coleman & Melville, 1994; Venditti *et al.*, 2005; Lin & Venditti, 2013). As such, there is good reason to suspect a relation between transport stage and migration rate.

A common measure of transport stage is the non-dimensional Shields stress divided by its value at the threshold for sediment entrainment or τ_*/τ_{*c}. The Shields stress is calculated as:

$$\tau_* = \frac{\tau}{(\rho_s - \rho_w)gD} \quad (1)$$

where τ is the shear stress at the bed, ρ_s and ρ_w are the sediment and water densities, respectively, g is gravitational acceleration and D is the grain size of the sediment, which is usually taken to be the median size D_{50} (Raudkivi, 1967). Values of the critical value of τ_* for sediment entrainment (τ_{*c}) vary with grain size (cf. Miller *et al.*, 1977; Yalin & Karahan, 1979b; Brownlie, 1981).

Church (2006) established ranges of τ_*/τ_{*c} for bedload dominated (BLD) conditions when $1 < \tau_*/\tau_{*c} < 3{\cdot}3$, mixed-load dominated (MXD) conditions when $3{\cdot}3 < \tau_*/\tau_{*c} < 33$ and suspended-load dominated (SSD) conditions when $\tau_*/\tau_{*c} > 33$. The BLD and SSD conditions were defined using the thresholds for motion and suspension, established empirically for reach-scales. The ranges were not intended to represent local particle dynamics. More useful boundaries for BLD, MXD and SSD conditions, that describe particle dynamics in terms of local flow conditions, can be derived from a common suspension threshold as the ratio of the shear velocity to the settling velocity, u_*/w_s whereby suspension occurs when $u_*/w_s > 1$ (e.g. Bagnold, 1966; Nino & Garcia, 1998; Lopez & Garcia, 2001). BLD conditions occur when $\tau_*/\tau_{*c} > 1$ and $u_*/w_s < 1$, MXD conditions occur when $u_*/w_s \geq 1$ and SSD conditions occur when $u_*/w_s \leq 1$. It is possible to recast this suspension threshold into a transport stage for a given sand size because Shields stress and the suspension criteria have the same basic form (a shear stress metric divided by a grain size metric) and $\tau_* \propto (u_*/w_s)^2$. This approach has the advantage of placing the threshold for motion into the same rubric as the threshold for suspension.

Yalin (1972) showed that bedform geometry changes with transport stage. Bedform aspect ratios (bedform height divided by length, H/L) are low when τ_*/τ_{*c} is just above 1, increases with transport stage under BLD conditions, are largest under MXD conditions and decline with increasing transport stage under SSD conditions, until they washout to a flat bed. Ripples and dunes follow the same pattern, but ripple H/L peaks at lower values of τ_*/τ_{*c}. Data compiled by van Rijn (1984, 1993) and perturbation theory proposed by Fredsoe (1982) both demonstrate similar patterns, but the functional forms of the relations are somewhat different. However, experiments designed to examine how bedform dimensions adjust to changes in transport stage, holding other factors that influence bedform dimensions constant, have not been undertaken. This is particularly concerning because there are relatively few observations of bedform dimensions under SSD conditions.

Recognizing the relations between transport stage, bedform dimensions and migration rates, Lin & Venditti (2013) examined the relation between transport stage and migration rates using data from a wide variety of laboratory flume experiments and field observations. For dune fields that are in equilibrium with an imposed flow, these authors demonstrated that migration rates increase with transport stage for a given grain size. The derived model between transport stage and translation rates holds across orders of magnitude of bedform size. Lin & Venditti (2013) also found that dunes move faster in coarser sediment than in finer sediment at a given transport stage, probably because finer sediment is more likely to bypass the crestline and not contribute to downstream migration (Mohrig & Smith, 1996). This implies that the suspension potential of the sediment is important for controlling translation rates.

The results of Lin & Venditti (2013) apply strictly to bedform translation rate, which is the downstream migration of bedforms without changes in the shape, size or spacing. McElroy & Mohrig (2009) show that the elevation change at

© 2015 The Authors. Sedimentology © 2015 International Association of Sedimentologists, *Sedimentology*

a point with time in a bedform field can be decomposed as:

$$\frac{\partial \eta}{\partial t} + V_b \frac{\partial \eta}{\partial x} + \delta_b = 0 \quad (2)$$

where η is the bed elevation, t is time, x is distance alongstream, V_b is the bedform migration rate and δ_b is the deformation rate of the bed. The first term on the left-hand side is the change in bed elevation at a point through time. The second term represents downstream translation of the waveform. Deformation is the sum of all changes to the topographic profile of the bed that are not associated with the downstream translation and may include changes in bedform shape, size and spacing. As such, deformation can represent an important component of bedform kinematics and bedform-related sediment flux. Surprisingly little is known about bedform translation and deformation in sand-bedded river channels and how they vary with transport stage, which may be problematic when examining bedform migration rates across a wide range of transport stages because McElroy & Mohrig (2009) reasoned that downstream bedform translation contributes to bedload transport in the channel while deformation contributes to the suspended load because, by definition, deformation occurs by vertical exchange of sediment between the bedform and the flow.

Here, bedform dimensions, morphodynamics and migration rates are examined experimentally under BLD, MXD and SSD conditions. Initial flow depth and bed material grain size were held constant because they are thought to be important controls on dune size and migration rates. Rather than a less detailed examination of many variants of the experimental conditions, which has been done before, three experimental runs are examined in detail. Answers to the following questions are sought: (i) how do bedform dimensions change with transport stage; (ii) how do bedform translation and deformation change with transport stage; and (iii) what is the relation between bedform translation, deformation, and the dominant transport modes?

METHODS

Laboratory experiments were conducted in the River Dynamics Laboratory (RDL) at Simon Fraser University, Canada. The RDL flume is 15 m long with a 12 m long working section, 1 m wide and 0·6 m deep, it has an adjustable slope (−0·5 to 2·0%) and can accommodate flows up to 0·2 $m^3\ s^{-1}$. The flume re-circulates water and sediment. Sediment used in the experiment was well-sorted quartz sand with D_{50} = 550 μm (Fig. 1). Mineralogical analysis showed that the sand was 99·9% quartz, with trace amounts (<0·1%) of sillimanite, garnet, sphalerite, muscovite and gold attached to quartz.

Experimental design and procedure

The experiment consisted of three runs under BLD, MXD and SSD conditions (Table 1), designed in consideration of the Church (2006) reach-scale ranges of τ_*/τ_{*c} for each transport stage and the values of u_*/w_s that would produce a given transport stage. Ultimately, the flow conditions were set based on visual observation of the modes of transport. The BLD run had no suspension; the SSD run had a substantial suspended component and was just at the threshold for the dunes washing out; the MXD run was above the threshold suspension. To ensure that a flow condition would produce dunes, the 10°C-equivalent mean velocity and grain size were calculated and compared to the bedform phase diagrams of Southard & Boguchwal (1990). The BLD, MXD and SSD conditions plot in the lower, middle and upper portions of the dune phase space (Lin, 2011).

The transport stage and u_*/w_s were calculated to ensure that they were reasonably close to the design values, τ_* was calculated by assuming ρ_w and ρ_s were 1000 kg m^{-3} and 2650 kg m^{-3}, respectively. The boundary shear stress was calculated from the depth-slope product:

$$\tau_o = \rho_w g h S \quad (3)$$

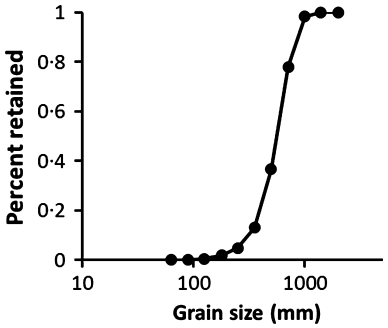

Fig. 1. Grain-size distribution of sediment used in experiments.

© 2015 The Authors. Sedimentology © 2015 International Association of Sedimentologists, *Sedimentology*

Table 1. Summary of flow parameters. BLD, bedload dominated conditions; MXD, mixed-load dominated conditions; SSD, suspended-load dominated conditions.

Parameter	BLD	MXD	SSD
Mean velocity, $\overline{U}$ (m s^{-1})	0·433	0·587	0·867
Mean flow depth, $\overline{h}$ (mm)	151	152	134
Froude number	0·36	0·48	0·76
Reynolds number	64 418	87 907	114 463
Slope, $S \times 10^{-3}$	1·32	3·37	6·13
Shear stress†, τ (Pa)	1·90	4·89	7·86
Shear velocity u_* (m s^{-1})	0·044	0·070	0·089
Design τ_*/τ_{*c}‡	4·23	20·4	35·1
Design u_*/w_s	0·252	1·21	2·09
Observed τ_*/τ_{*c}‡	7·13	18·3	29·7
Observed u_*/w_s	0·657	1·04	1·33

†Sidewall corrected using Williams (1970).
‡Calculated for 0·55 mm sand using $\tau_{*c} = 0{\cdot}03$ (van Rijn, 1993).

where h is flow depth and S is the water surface slope. This calculation represents the sum of the grain-related and bedform-related shear stress. Sidewall corrections were implemented to calculate the shear stress applied to the bed using the empirical equation of Williams (1970):

$$\tau = \frac{\tau_o}{(1 + 0{\cdot}18h/w^2)} \quad (4)$$

where w is the width of flume. The shear velocity was calculated as $u_* \equiv \sqrt{\tau_o/\rho}$ and w_s was calculated using Dietrich (1982). Flow depth was held constant at *ca* 0·15 m, by filling the recirculating flume to the desired depth. The slope was then adjusted to the design value and the flow depth adjusted independently to the imposed slope when the pumps were started (Table 1). Dune H and L are influenced by flow depth, so by holding the depth approximately constant, the observed variation in morphology is due to changes in the transport modes.

After the desired h and S were set for a given run, the flume was allowed to run until an equilibrium was reached where S and h became constant (slope of the time series of h and S approached zero) and the bedforms were fully adjusted to the flow condition. This process took 72 h prior to the BLD and MXD runs and 30 h prior to the SSD run. After reaching equilibrium conditions, each run was approximately 18 h, over two days. The flume was shut down at the end of each day, but the bed was left fully submerged to ensure negligible effect of the interruption. The data showed no evidence of the interruption on the bed morphology.

Bed and water surface measurements

Observations were made using a Swath Mapping System (SMS; Fig. 2) that measured alongstream profiles of bed topography and water surface elevation. The SMS consists of: (i) a 32 transducer Seatek echo-sounding system (Seatek Inc., Gainesville, FL, USA); (ii) three MassaSonic ultrasonic sensors (Massa Products Corporation, Hingham, MA, USA); (iii) a mechanical stepper-motor driven arm that moves sensors vertically; (iv) a mechanical, stepper-motor driven system that moves the SMS in the streamwise direction; and (v) an onboard computer that records all sensor signals and positions. The SMS traverses the flume on rails attached to the top of the tank (Fig. 2).

The Seatek transducers are mounted in a Plexiglas® beam (Fig. 2) that is submerged a few millimetres below the water surface to measure bed elevations. When the SMS is moving downstream, the rate of movement and sampling frequency determines measurement point density, and the sampling frequency is dependent on the number of transducers sampled. Sixteen odd-numbered (1, 3, 5 ... 31) transducers were sampled during each pass over the bed producing parallel profiles of bed topography with measurements at 0·5 mm intervals in the alongstream x-direction. The alongstream profiles were spaced at 61 mm in the cross-stream y-direction. The profile from transducer 17 is closest to the centre of the channel at 486 mm from the right-hand flume wall, looking downstream. The ultrasonic sensors (Fig. 2) measure the water surface elevation at y-positions of 206 mm, 499 mm and 805 mm from the right flume wall.

Measurements of bed and water surface topography along at least 6 m of the flume (streamwise direction) were made with the SMS every 10 min during the BLD and MXD runs. The period between SMS measurements was decreased to every 5 min during the SSD run because the bed evolved so quickly. The speed of the SMS was also increased during the SSD run to decrease the time when the Plexiglas bar dis-

© 2015 The Authors. Sedimentology © 2015 International Association of Sedimentologists, *Sedimentology*

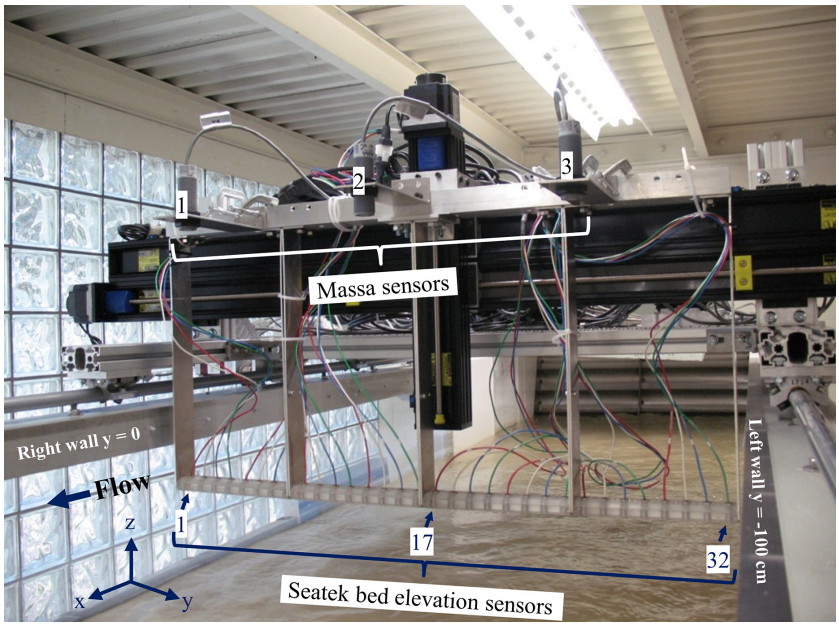

Fig. 2. The Swath Mapping System (SMS).

turbed the water surface, decreasing the alongstream distance between raw measurements to *ca* 4·5 mm.

Sediment transport measurements

Suspended-sediment samples were collected with a syphon system composed of an L-shaped copper tube, a nylon tube and a variable speed peristaltic pump. The syphon sampler was mounted on a point gauge to position it in the flow. The point gauge was incremented at 0·3 mm. Samples were taken at 40 mm above the bed in the centre of the channel over dune crests. While suspended-sediment flux may vary along the dune profile due to deposition in the bedform trough and resuspension over the dune stoss slope, erosion and deposition should be balanced at the dune crest, making this the least biased position from which to take suspended-sediment flux measurements. In order to make the system isokinetic, the pump rate was calibrated to the calculated flow velocity at the intake by assuming a logarithmic velocity profile over the dune crests. Samples were filtered using glass microfibre filters with a pore size of 1·6 μm to obtain sediment concentrations.

The suspended-sediment flux was calculated using the Rouse equation (Rouse, 1939):

$$\frac{C}{C_a} = \left(\frac{h-z}{z}\frac{a}{h-a}\right)^{\frac{w_s}{\beta\kappa u*}} \quad (5)$$

where C is the concentration of suspended-sediment at height z above the sediment bed, C_a is a reference concentration measured at elevation a = 40 mm above the bed, β is a coefficient that describes the difference in diffusion between a sediment particle and a fluid particle (assumed to be 1), κ is the von Karman constant (0·41) and $u*$ is the shear velocity calculated as $(\tau/\rho_w)^{0.5}$. Suspended-sediment flux per unit width is calculated as:

$$q_{ss} = \overline{U} \times \overline{C}h \quad (6)$$

where $\overline{U}$ is the mean streamwise velocity and the overbar indicates a depth-average. Calculation of q_{ss} as the product of mean velocity and mean concentration can induce a bias in the flux when compared to the mean of the velocity-concentration product (i.e. $\overline{UC}$) but the resultant bias is negligible for the present conditions.

A small amount of fine silt present in the bed sediment made up ≪1% of the bed material which, once entrained in the flow, remained in suspension. After a series of bedforms had passed through the flume, the concentration of silt suspended in the flow was approximately constant. Values of q_{ss} were corrected by mea-

© 2015 The Authors. Sedimentology © 2015 International Association of Sedimentologists, *Sedimentology*

suring this washload concentration at the BLD transport stage, where the only sediment in suspension was the fine silt, and subtracting it from measured concentrations at all transport stages.

Bedload flux was measured with miniaturized Helley-Smith samplers (Helley & Smith, 1971) that were scaled down to a 20 mm square mouth (Fig. 3A; Dietrich & Smith, 1984; Mohrig & Smith, 1996) with a 75 μm mesh bag. The samplers were mounted such that one sampler collected sediment moving within the bottom 20 mm of the flow and the other collected sediment between 20 mm and 40 mm above the bed (Fig. 3A). Bedload samples were collected in sets of three over bedform crests (Fig. 3B) at the downstream end of the bed topography measurement section. The bedload flux over the dune crest is delivered to the lee side, which causes downstream migration, making this the best place to estimate bed material bedload transport associated with the dune. Some sample sets did not contain samples from all three samplers either because the operator could not identify a sampling spot or because placement of the sampler substantially altered the dune crest. Bedload flux q_{bl} was calculated as the average of sample weights across the channel, divided by the sample times of a set. Observations from the top samplers are not presented, because isokinetic suspended samples are a more reliable method for measuring suspended-sediment flux.

The Helley-Smith samples included bedload (material transported in traction and saltation), as well as material carried in intermittent suspension near the bed because the bedload trap measured all sediment travelling between the bed and $z = 20$ mm. Therefore, the Helley-Smith samples are biased at the MXD and SSD transport stages where there was substantial bed material suspension. Measured bedload flux was corrected by calculating the height of the saltation layer using a model from van van Rijn (1984). The Bagnold (1973) and Sklar & Dietrich (2004) saltation height models produce nearly identical values to the van Rijn (1984) model over the range of conditions in the experiment. A linear vertical concentration profile was assumed, from the bed to $z = 20$ mm, and the Helley-Smith measurements were split into bedload and suspended load, the latter of which was added to q_{ss} calculated using Eq. 6 to get the total suspended bed material flux. More complicated, nonlinear profile shapes (for example, Eq. 5) were examined, but the different profile shapes produce very similar corrections.

Data analysis

Bed surface data were filtered to remove acoustic noise using a three-step process:

1 A filter removed elevations that were obviously noise (values below the Plexiglas flume floor and 0·18 m above the flume floor (near the water surface).

2 A 20 point running average of elevation was calculated and elevation readings that exceeded the average value by 3 mm or were less than the

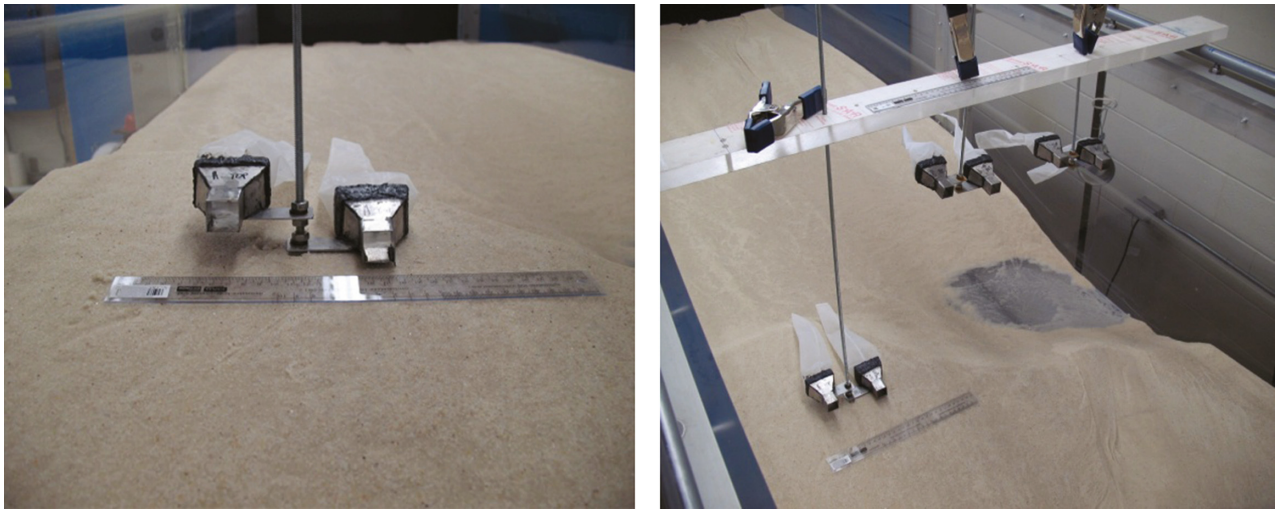

Fig. 3. Miniaturized Helley-Smith samplers constructed by the authors.

© 2015 The Authors. Sedimentology © 2015 International Association of Sedimentologists, *Sedimentology*

average value by 1 mm were removed. These values were not replaced.

3 Step 2 was repeated, but all removed values were replaced by the local mean, effectively smoothing the profile.

The reason for the difference in the filtering thresholds for Steps 2 and 3 has to do with the bottom detection algorithm used by the Seatek manufacturer. It was found that the echo-sounders were more prone to falsely identifying the bottom as being above the bed than below, so the filtering was adjusted accordingly. Comparison of the filtered and unfiltered data showed that the process was effective at removing noise, but did not affect the dune shape. The same process was used to filter the water surface elevation profiles.

Water surface slope was calculated as the sum of the water surface slope relative to the flume tank, measured using alongstream profiles, and the slope of the flume tank. The latter was measured with an electronic height gauge mounted to the flume and the laboratory floor that has a resolution of 0·01 mm, but a practical resolution of 0·1 mm.

Bedform dimensions were calculated from the filtered bed profiles using both a manual and an automated method, which are compared here. The manual method used detrended, alongstream bed profiles obtained along the channel centreline. Heights were measured from the peak to the trough in the lee side of each bedform. Reported height H is the mean for an alongstream transect. Bedform lengths L were measured for a profile by measuring the total distance of a train of bedforms and dividing by the number of bedforms. As such, it also is a mean value for an alongstream transect. Bed elevation changes <10 mm and lengths <0·3 m were omitted from the calculations of H and L to keep the work tractable. This omission constrained the analysis to larger scale bedforms, excluding smaller scale, superimposed bedforms and perturbations in the bedform field, both of which were observed.

This manual method produced statistics for the channel centreline, but was too labour intensive to pursue for all 16 alongstream profiles, so an automated method, developed by McElroy (2009) was also used. This permitted the calculation of spatial averages of bedform dimensions. The standard deviation of detrended alongstream profiles of bed elevation was calculated as:

$$W(l) = \left[\frac{1}{n}\sum_{i=1}^{n}(\eta_i - \overline{\eta})^2\right]^{0.5} \quad (7)$$

for a continuous range of bed profile lengths l to produce a function that increases asymptotically (n is the number of bed elevations in an alongstream bed profile, η is the bed elevation and the overbar represents an average over l). The value of l when the $W(l)$ curve approaches the asymptote defines a 'saturation length' L_{sat}. In order to estimate L_{sat} unambiguously, McElroy (2009) calculates a new curve that is the logarithmic derivative of $W(l)$. The saturation length is taken as the value of l when the logarithmic derivative of $W(l)$ is half the value of the first peak in the curve. A 'characteristic bedform length' L_c for an alongstream profile can be calculated from L_{sat} as:

$$L_c = \frac{\pi L_{sat}}{2} \cong 1 \cdot 57 L_{sat} \quad (8)$$

McElroy (2009). The corresponding value of $W(l)$ at L_{sat} defines a 'saturation height' H_{sat} that can be used to calculate a 'characteristic bedform height' as:

$$H_c \cong 2 \cdot 8 H_{sat} \quad (9)$$

McElroy (2009). In order to apply the method, bed profiles linearly interpolated to a 0·5 mm spacing were used.

Bedform translation rates were also obtained with a manual method and an automated method. Both methods used consecutive alongstream bed elevation surveys separated by some time interval. In the manual method, bedforms were identified in both surveys and the translation distance was measured using alongstream profiles from the centre Seatek sensor. When a bedform in the earlier survey split into two smaller bedforms in the later survey, the nearest downstream crest in the later survey was selected to calculate the translation distance. However, when two bedforms in the earlier survey merged into a single bedform in the later survey, the crest further upstream in the earlier survey was used. Some bedforms changed their geometry instead of changing in streamwise position and their translation distance was set at zero. This method was not performed on profiles from the SSD run because bedform shape changed so much between two consecutive surveys,

© 2015 The Authors. Sedimentology © 2015 International Association of Sedimentologists, *Sedimentology*

it was not possible to reliably match them by eye.

The automated method calculated translation distance using autocorrelation of two consecutive alongstream profiles that were linearly interpolated at a spacing of 1 mm. The profiles were lagged relative to one another and coefficient of determination (r^2) was calculated for each lag distance. The profiles were lagged 1 to 1000 times (up to 1 m) for BLD, 1 to 1500 times (up to 1·5 m) for MXD, and 1 to 3000 times (up to 3 m) for SSD conditions. Translation distance between two surveys was taken as the lag distance that corresponded to the maximum r^2 value. As a quality control measure for the SSD condition, a lag of 5000 steps (5 m) was also used. If the lag distance was different between 3000 and 5000 steps, the profiles were deemed too different to reliably calculate a translation distance. This automated method produced a translation distance for all 16 alongstream profiles in a survey, which were then averaged and divided by the survey interval to get a spatially-averaged translation rate for the survey.

RESULTS

The flume slope, initial water depth and channel discharge were imposed in the experiment, but the water surface slope, depth and transport stage adjusted to these initial conditions. Flow depth remained at *ca* 0·15 m for the BLD and MXD transport stages but dropped to 0·134 m at the SSD transport stage (Table 1). The observed transport stages deviated from the design values slightly. The water surface slope relative to the flume was assumed to be negligible during the BLD run, but subsequent analysis revealed that this was not true and that τ_*/τ_{*c} was actually 1·7 times greater than the design value (Table 1). The observed τ_*/τ_{*c} for the SSD transport stage is 14% less than the design value because the depth declined in response to the flow (Table 1). However, visual observations of sediment movement at each transport stage were consistent with BLD, MXD and SSD conditions. Furthermore, the BLD condition is below the threshold for suspension (u^*/w_s = 0·66); the MXD condition is just above the threshold of suspension (u^*/w_s = 1·04); the SSD condition well exceeds the threshold (u^*/w_s = 1·33).

Variability in S, h and τ_*/τ_{*c} increased slightly from BLD to MXD transport stages, but increased dramatically from the MXD to SSD transport stages (Fig. 4). This pattern of variability is mirrored in the bedform dimensions and translation rates. The sampled sediment transport rates are summarized in Table 2 and the calculated q_{bl},

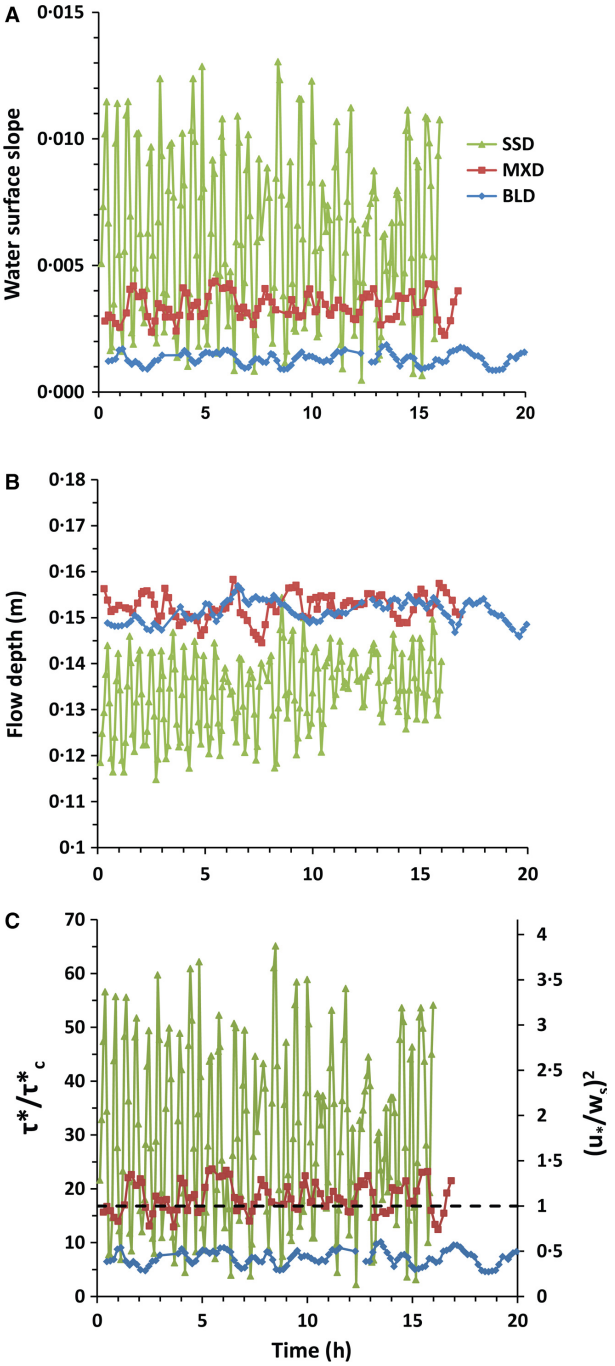

Fig. 4. Time series of water surface slope, flow depth, transport stage (τ_*/τ_{*c}) and the ratio of the shear velocity to the settling velocity (u_*/w_s) for the BLD, MXD and SSD conditions. The dashed line indicates the suspension threshold u_*/w_s = 1. BLD, bedload dominated conditions; MXD, mixed-load dominated conditions; SSD, suspended-load dominated conditions.

© 2015 The Authors. Sedimentology © 2015 International Association of Sedimentologists, *Sedimentology*

Table 2. Sampled sediment transport rates; n, number of sampling sets.

	Helley-Smith		Syphon		
	n	Mean (g sec^{-1} m^{-1})	*n*	Mean (g sec^{-1} m^{-1})	Depth-integrated suspended bed material load (g sec^{-1} m^{-1})
Bedload dominated conditions (BLD)	24	25·8	15	0·759	0
Mixed-load dominated conditions (MXD)	21	111	17	8·10	7·06
Suspended-load dominated conditions (SSD)	23	459	18	76·7	75·4

q_{ss} and total bed material flux $q_s = q_{bl} + q_{ss}$ are given in Table 3. Both bedload and suspended bed material flux increased with transport stage. At the BLD stage, q_s is equivalent to q_{bl}. At the MXD and SSD transport stages, q_{bl} is *ca* 30% of q_s.

Although there was clearly more material in suspension during the SSD run than the MXD run, it is difficult to distinguish the runs based on the ratio of suspended-sediment flux to the total flux. In fact, q_{ss}/q_s was slightly higher in the MXD run than in the SSD run. With a narrowly graded sand, it is not possible to generate a condition where suspended bed material dominates over bedload flux and retains bedforms, because as the suspended bed material load increases, so does the bedload.

Bedform morphodynamics

Bedload dominated transport stage

At the BLD transport stage, sediment moved in contact or within a few grain diameters of the bed and transport was generally patchy and intermittent. Although the occasional grain was suspended from bedform crests, there was no measureable bed material suspension (Table 3). Figure 5A to C shows the bed topography for three consecutive bed surveys and the change in bed elevation $\Delta\eta$ between the surveys (Fig. 5D and E). The bedforms were angle of repose, asymmetrical bedforms, commonly observed in small channels and flumes, as opposed to the larger scale low lee angle dunes typically observed in large river channels (cf. Kostaschuk & Villard, 1996; Bradley *et al.*, 2013). The three-dimensional bedforms had mean heights of *ca* 45 mm and mean lengths of *ca* 0·9 m. Saddle-shaped portions of crestlines formed downstream of lobe-shaped crestlines along with spurs (ridges parallel to the flow; Fig. 5A to C). There were some sandsheet features (cf. Venditti *et al.*, 2005) superimposed on the backs of the larger bedforms. Bedform troughs were more deeply scoured at the flume walls, presumably due to increased wall drag.

The change in topography between the surveys is not great (Fig. 5D and E). The bedform shapes did evolve, but they are readily identifiable from one survey to the next (Fig. 5A to C). The irregular patterns in $\Delta\eta$ (Fig. 5D and E) highlight the effect of bedform three-dimensionality on migration rates. Lobe-shaped portions of crestlines moved faster than saddle-shaped portions of the crest. Lobes were observed to catch up with the slower moving saddle shapes, forming a new lobe at the sides of the pre-existing lobe or saddle, contributing to the change in bedform shape. Ridges sometimes shifted from side to side, also contributing to alongstream bedform profile change, but not contributing substantially to downstream bedform translation.

Mixed-load dominated transport stage

Sediment was readily entrained into suspension during the MXD transport stage (Table 3), bypassing the dune crestline, and the morphodynamics of the bedforms reflect this behaviour. Figure 6A to C shows a series of bed elevation surveys and $\Delta\eta$ calculated between surveys (Fig. 6D and E). The bedforms had the same morphological characteristics as at the BLD stage: angle of repose, asymmetrical, three-dimensional features composed of lobes, saddles and spurs, but the bedforms are higher (*ca* 65 mm) and longer (*ca* 1·3 m). The increase in height appears to be due to deeper scour in the trough. Sandsheets migrating over the backs of dunes are readily identifiable over the larger bedforms (Fig. 6A to C). Bedform crests became rounder and the lee slopes were more gentle, but the slipface slopes remained at approximately the angle of repose. Comparing Fig. 5A to C with Fig. 6A to C, it appears that the bedforms were higher because of

© 2015 The Authors. Sedimentology © 2015 International Association of Sedimentologists, *Sedimentology*

Table 3. Corrected sediment transport rates. Values in brackets are the coefficient of variation. BLD, bedload dominated conditions; MXD, mixed-load dominated conditions; SSD, suspended-load dominated conditions.

	q_{bl} (g sec^{-1} m^{-1})	q_{ss} (g sec^{-1} m^{-1})	q_s (g sec^{-1} m^{-1})	$\overline{q_{T-m}}$ (g sec^{-1} m^{-1})	$\overline{q_{T-a}}$ (g sec^{-1} m^{-1})	$\overline{\langle q_{T-a} \rangle}$ (g sec^{-1} m^{-1})	q_D (g sec^{-1} m^{-1})	q_T/q_D	q_T/q_{bl}	q_D/q_{ss}
BLD	25·8	0	25·8	14·4 (31·4)	13·5 (29·7)	12·4 (17·3)	13·4	0·925	0·481	∞
MXD	34·9	83·6	119	53·5 (50·6)	60·1 (42·4)	67·6 (23·2)	51·4	1·32	1·94	0.615
SSD	178	357	535	159[‡] (54·1)	166[‡] (51·8)	156[†,‡] (38·8)	379	0·412	0·876	1.06

[†]There is no manual bedform velocity, so the automated bedform velocity from the channel centreline was substituted, filtered to remove any negative velocities and V_b values that were different between the 3 m and 5 m windows. [‡]Based on the final 8 h of the experiment due to unsteadiness in the height time series.

deeper troughs, presumably caused by more vigorous mixing in the bedform lee during the MXD run.

The change in topography between the surveys was greater than at the BLD stage (Fig. 6D and E). Once the bedforms had migrated about one wavelength, it became difficult to identify the same features between surveys (Fig. 6A to C) because of greater bedform merging and splitting. There are obvious bands of larger $\Delta\eta$ in Fig. 6E and D that represent bedform translation, but there are also a wider range of bed elevation changes than during the BLD run, in part because the bed was evolving more quickly between surveys.

Suspended-load dominated transport stage

At the SSD transport stage, the bedload layer became deeper and the flux rates increased substantially compared to the BLD and MXD runs (Table 3). Figure 7A to C shows that the bedform morphology became unstable and it was difficult to track individual bedforms, but scoured troughs did persist. Through time, the bed appeared to alternate through three phases: (i) plane bed with washed-out dunes (Fig. 7C); (ii) a train of large dunes (Fig. 7B); and (iii) a train of small dunes (Fig. 7A). In Phase 1, the bed was mostly flat and bedforms had lengths ranging from 1·5 to 2·5 m and heights ranging from 20 to 50 mm. Some bedforms were as high as 80 mm. In Phase 2, the bed was populated by large bedforms up to 100 mm in height and 3 m long. In Phase 3, the bed was populated by bedforms less than 1 m long and 20 to 40 mm high.

Visual observations by the present authors suggest that the transition between these phases was continuous rather than punctuated. In Phase 1, flow separation and localized, intense erosion occurred on extended flat areas of the bed, forming bedforms observed in either Phase 2 or 3. Transition occurred by formation of a localized incision, often followed by evenly spaced incision events upstream and downstream of the initial incision. In Phase 2, large dunes emerged that often split into smaller dunes forming Phase 3 and the smaller dunes characteristic of Phase 3 often combined to form the large dunes of Phase 2. Dune fields in Phase 2 or 3 would sometimes wash out to the nearly flat bed of Phase 1, which would then be dissected again. The time a phase existed varied from a few minutes to more than half an hour. Transformation between phases could occur

© 2015 The Authors. Sedimentology © 2015 International Association of Sedimentologists, *Sedimentology*

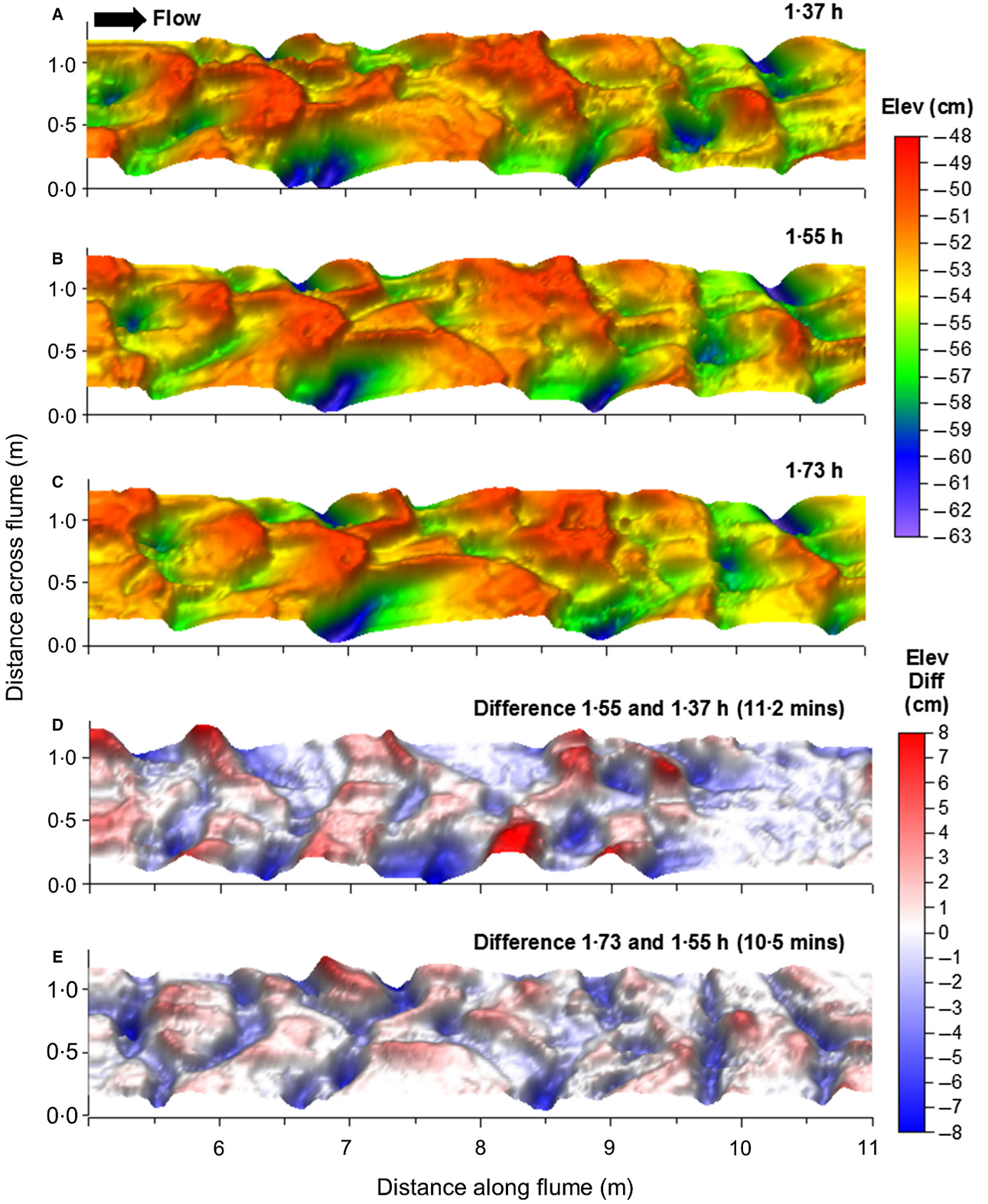

Fig. 5. Bed topography and elevation change at the bedload dominated transport stage.

© 2015 The Authors. Sedimentology © 2015 International Association of Sedimentologists, *Sedimentology*

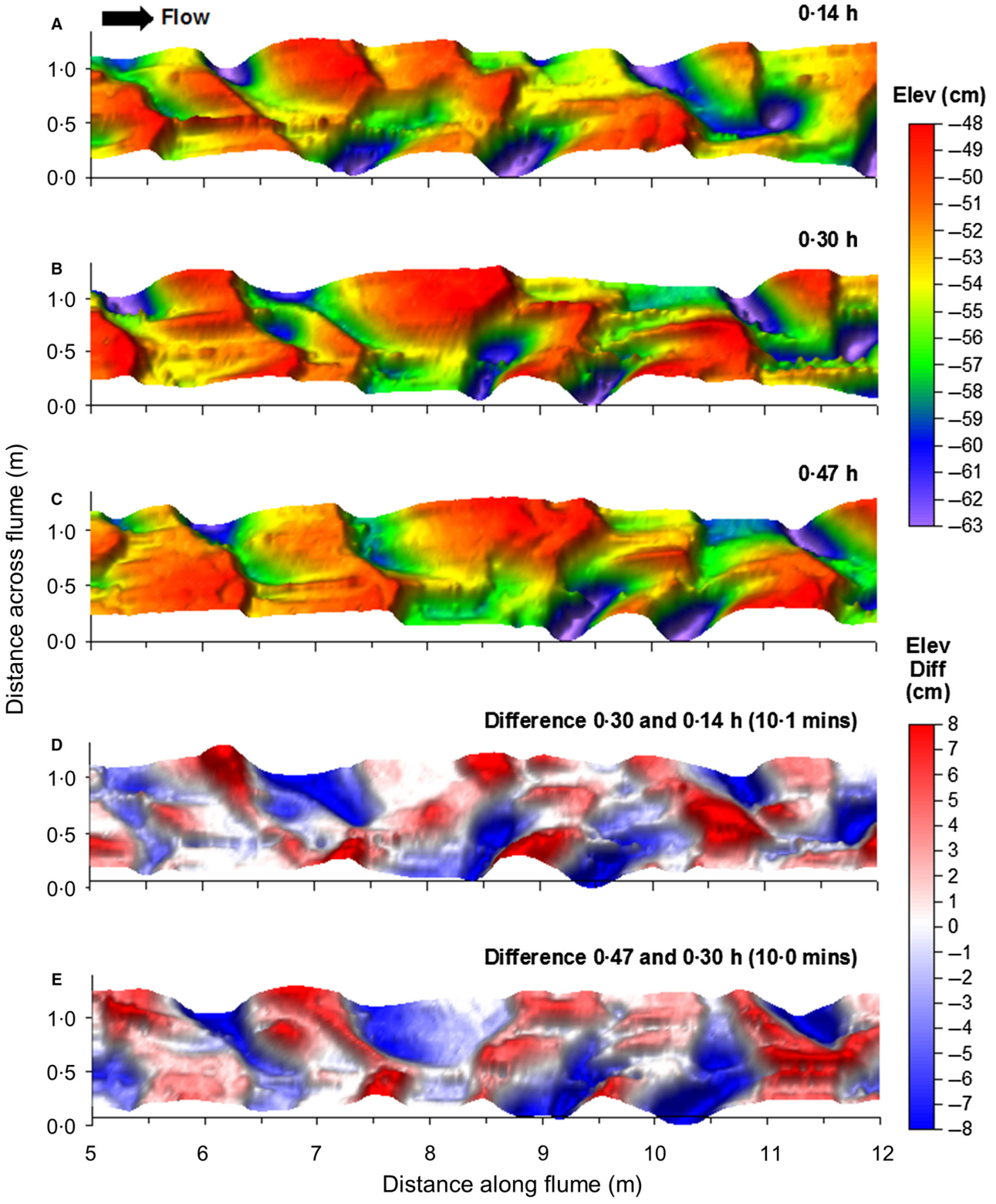

Fig. 6. Bed topography and elevation change at the mixed-load dominated transport stage.

over a few seconds or minutes. Washed-out, low-amplitude bedforms existed for longer than the small and large dune phases. This pattern of bedform evolution resulted in longer and lower amplitude bedforms (Fig. 7A to C). Sediment by-passed the crest moving into suspension and

© 2015 The Authors. Sedimentology © 2015 International Association of Sedimentologists, *Sedimentology*

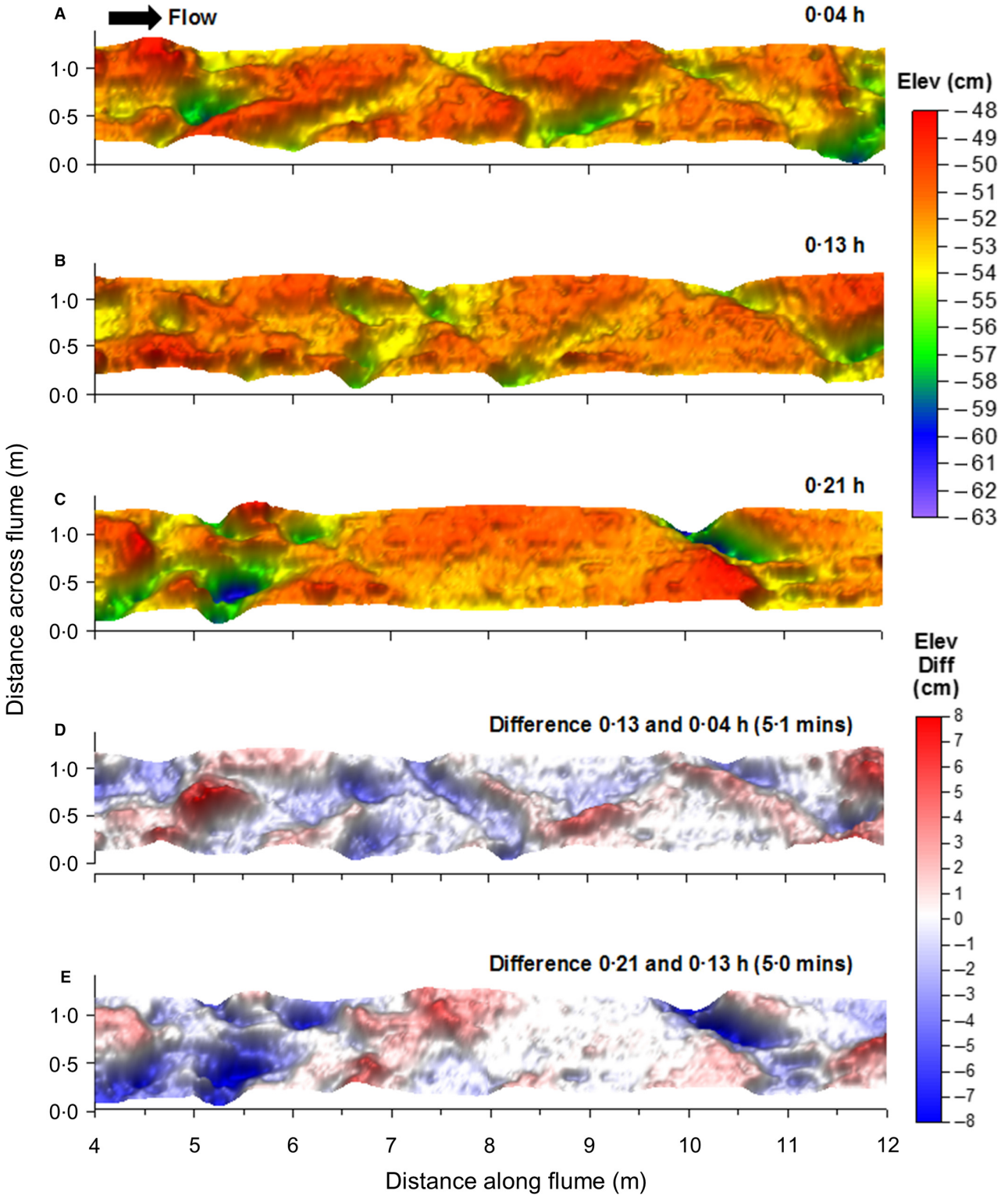

Fig. 7. Bed topography and elevation change at the suspended-load dominated transport stage.

bedform crests were round with lee slope angles lower than in the MXD run. Slipface slopes were approximately at the angle of repose, but they occupied short sections of the lee face. Angle of repose asymmetrical bedforms existed but were typically washed out quickly. Maps of

© 2015 The Authors. Sedimentology © 2015 International Association of Sedimentologists, *Sedimentology*

$\Delta\eta$ (Fig. 7D and E) are difficult to interpret because each phase represents a complete rearrangement of the bedform field.

Bedform dimensions

Method comparison

Figure 8 shows comparisons between the manual method for estimating bedform height and length (H_m and L_m) with the automated methods (H_c and L_c) along the channel centreline. The automated method yielded larger H and L values than the manual method at all transport stages. The manual measurements are regarded as more reliable measures of H and L because they are direct measurements of observed waveforms. The reliability of the automated measurements is not known, so deviations from H_m and L_m are treated as a bias inherent to the method. The bias in H_c relative to H_m is remarkably consistent, but declines slightly with transport stage: $\overline{H_c}/\overline{H_m}$ is 1·29, 1·26 and 1·23 for the BLD, MXD and SSD runs, respectively. The present sample size of three is too small to determine whether this pattern is real. The bias in L_c is less, but also consistent for the BLD and MXD runs where $\overline{L_c}/\overline{L_m}$ is 1·07 and 1·09, respectively. The bias is somewhat larger for the SSD run because *ca* 10% of L_c are >3 m, the maximum manually measured L_m. In these cases, the curve described by Eq. 7 did not reach an asymptote that corresponds to the bedform lengths due to residual trends in the bed profiles after linear detrending. Excluding these values, $\overline{L_c} = 1{\cdot}05\overline{L_m}$ for the SSD run.

The overestimation of H_m and L_m by the automated method along the channel centreline is a curious result, but is consistent with the results of McElroy (2009). The manual method is inherently biased towards larger bedforms because bed elevation changes smaller than 10 mm in height and 300 mm in length were ignored. The automated method is inherently biased towards smaller heights and lengths, assuming that there is a continuous distribution of bed elevations below the largest dunes. Nevertheless, the consistency of the overestimation of H_m and L_m by the automated method suggests that it can be corrected for by dividing H_c by 1·26 and L_c by 1·07, the mean overestimation ratio across all three runs, before calculating the spatial averages.

Spatially-averaged bedform dimensions

Figure 9 shows spatial averages of bedform height $\langle H_c \rangle$ and length $\langle L_c \rangle$, calculated using the McElroy (2009) method, corrected for bias. There is some minor non-stationarity in $\langle H_c \rangle$ and length $\langle L_c \rangle$, but the change in H or L is generally on the order of the instrument resolution

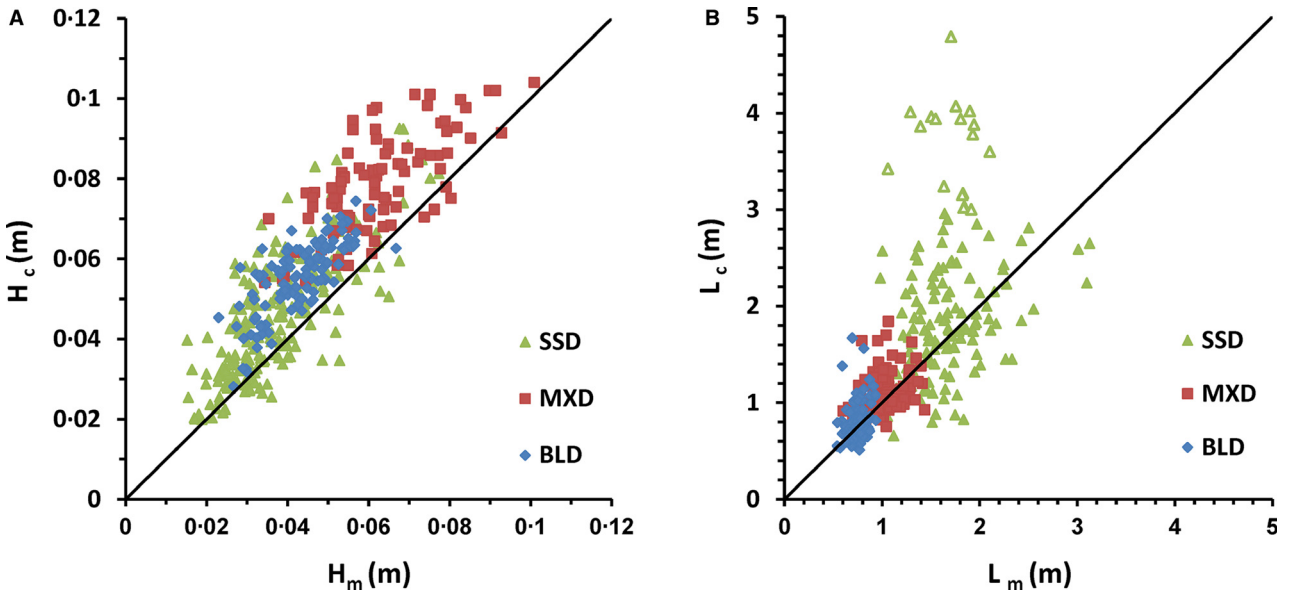

Fig. 8. Comparison between (A) bedform heights and (B) bedform lengths obtained along the channel centreline using the manual method (H_m and L_m) and the automated method (H_c and L_c) of McElroy (2009). Open triangles are L_c >3 m. SSD, suspended-load dominated conditions; MXD, mixed-load dominated conditions; BLD, bedload dominated conditions.

© 2015 The Authors. Sedimentology © 2015 International Association of Sedimentologists, *Sedimentology*

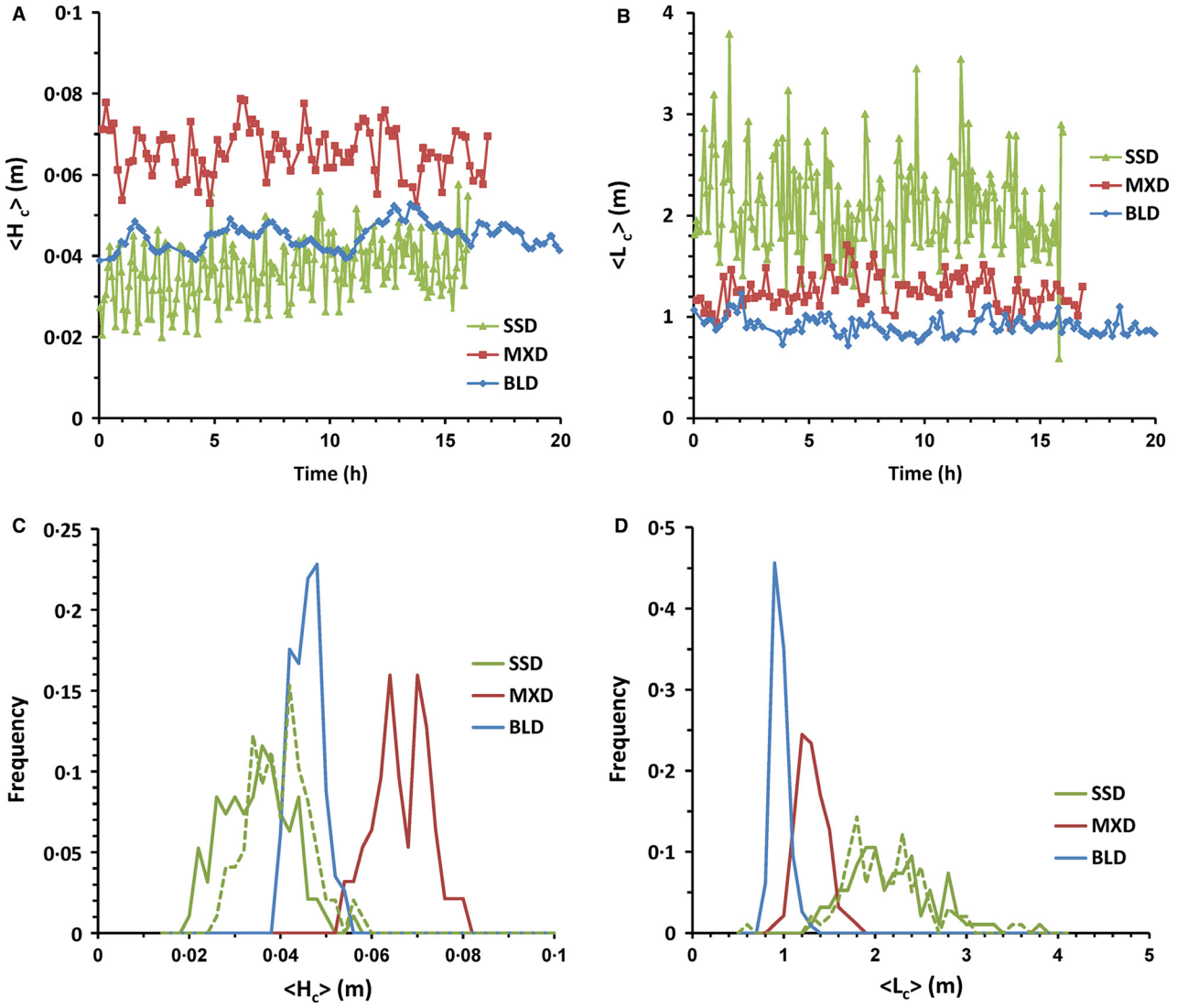

Fig. 9. Time series of spatially averaged bedform (A) height $<H_c>$ and (B) length $<L_c>$ and histograms of (C) $<H_c>$ and (D) $<L_c>$. The solid and dashed lines in panels (C) and (D) are for the first and last 8 h of the SSD run, respectively. SSD, suspended-load dominated conditions; MXD, mixed-load dominated conditions; BLD, bedload dominated conditions.

at the BLD and MXD transport stages and so is ignored. The non-stationarity in $<H_c>$ is more substantial at the SSD transport stage (Fig. 9A). Bedforms grew by *ca* 10% of the mean in the first half of the experiment, which had some impact on the distribution of sizes (Fig. 9C). The change in H was on the order of the instrument resolution during the second half of the experiment. The mean and median are *ca* 5 mm greater in the second half of the experiment compared to the first half. It is difficult to determine whether the increase in H was an adjustment towards equilibrium or simply related to the morphodynamics of a rapidly evolving bed, so the first 8 h of the experiment are removed from all further analysis. There is also some unsteadiness in the L time series at the SSD transport stage (Fig. 9B), but the distributions, mean and median are nearly identical between the first and second half of the experiment (Fig. 9D). Nevertheless, those L data are also removed from further consideration to be consistent with the H data.

The results show that H increased then decreased with transport stage (Fig. 9A; see Table 4 for mean values). The level of variability, quantified by the coefficient of variation (standard deviation divided by the mean), increases

© 2015 The Authors. Sedimentology © 2015 International Association of Sedimentologists, *Sedimentology*

Table 4. Mean bedform characteristics at different transport stages. Values in brackets are the coefficient of variation (%). BLD, bedload dominated conditions; MXD, mixed-load dominated conditions; SSD, suspended-load dominated conditions.

	$\overline{\langle H_c \rangle}$ (mm)	$\overline{\langle H_c \rangle}/h$	$\overline{\langle L_c \rangle}$ (m)	$\overline{\langle L_c \rangle}/h$	$\overline{\langle H_c \rangle}/\overline{\langle L_c \rangle}$	$\langle V_{bc} \rangle$ (10^{-4}; m s^{-1})
BLD	44·8 (7·2)	1/3·4	0·906 (9·9)	6·0	0·0498 (10)	3·09 (15)
MXD	65·7 (9·1)	1/2·3	1·26 (13·0)	8·3	0·0529 (11)	11·7 (18)
SSD*	38·8 (17)	1/3·5	2·06 (22·0)	15	0·0196 (27)	45·5 (36)

*Based on the final 8 h of the experiment due to unsteadiness in the height time series.

with transport stage (Table 4). The distribution of H is more peaked and narrow for the BLD run than for the MXD and SSD runs, which have similar shapes (Fig. 9C). Bedform lengths increased with transport stage from the BLD to the SSD transport stages (Fig. 9B; Table 4) as did the level of variation (Fig. 9D). Bedform aspect ratios were typical of dunes ($L \approx 20\ H$) at the BLD and MXD transport stages, but much lower at the SSD transport stage ($L \approx 57\ H$).

Bedform translation rates

Method comparison

Figure 10 compares the automated method used to estimate bedform translation rates (V_{bc}) with the manual method V_{bm}. The automated method should be a more reliable estimator of V_{bm} because the whole profile translation is measured, rather than select bedforms. There is no obvious bias in Fig. 10, but $V_{bc} = 0{\cdot}92\ V_{bm}$ for the BLD run and for $V_{bc} = 1{\cdot}13\ V_{bm}$ the MXD run. No comparison between V_{bc} and V_{bm} for the SSD run is presented because there was too much uncertainty in manually tracking bedform crests. Given the similarity between V_{bc} and V_{bm} and that the calculated bias is not consistent, no corrections are made to V_{bc}.

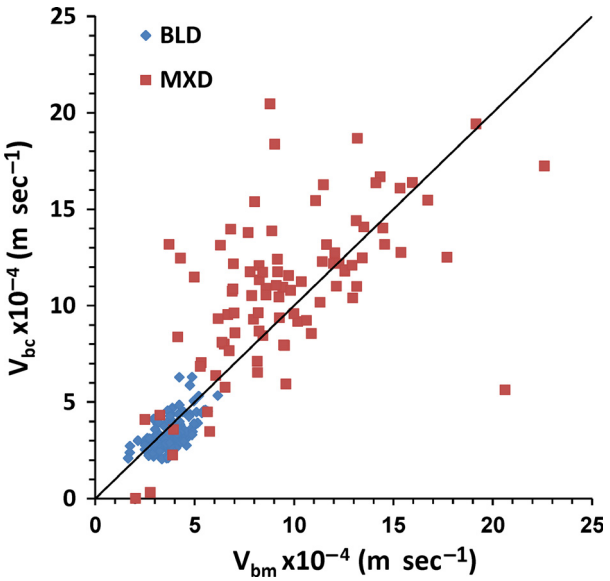

Fig. 10. (A) Bedform translation rates obtained using the manual method (V_{bm}) and the automated method (V_{bc}) along the channel centreline. BLD, bedload dominated conditions; MXD, mixed-load dominated conditions.

Spatially averaged bedform translation rates

Figure 11 shows spatially averaged bedform migration rates $<V_{bc}>$ for each run. The time series are stationary, all increasing by <1% of the mean over the experiment. Migration rate increases with transport stage, as does the level of variability (Fig. 11A; Table 4). The distributions of $<V_{bc}>$ go from being narrow and peaked at the BLD stage to very broad for the SSD transport stage (Fig. 11B). This reflects the morphodynamics of the bedforms. Although the time series are stationary, $<V_{bc}>$ values from the first half of the SSD experiment are removed from further consideration to be consistent with the bedform dimension data.

Bedform-related sediment flux rates

Bedform translation flux rates

Sediment flux associated with translation is calculated using the Simons *et al.* (1965) approach:

$$q_T = \beta_b(1-p)V_b H \tag{10}$$

where p is the porosity of the bed (0·4) and β_b is a bedform shape factor equivalent to:

$$\beta_b = HL/A_b \tag{11}$$

where A_b is the cross-sectional area of the bedform (Venditti *et al.*, 2005). If the bedform is triangular, as assumed in the Simons *et al.* (1965) derivation, $\beta_b = 0{\cdot}5$. However, values of 0·56 are typical of asymmetrical bedforms (Van den Berg,

© 2015 The Authors. Sedimentology © 2015 International Association of Sedimentologists, *Sedimentology*

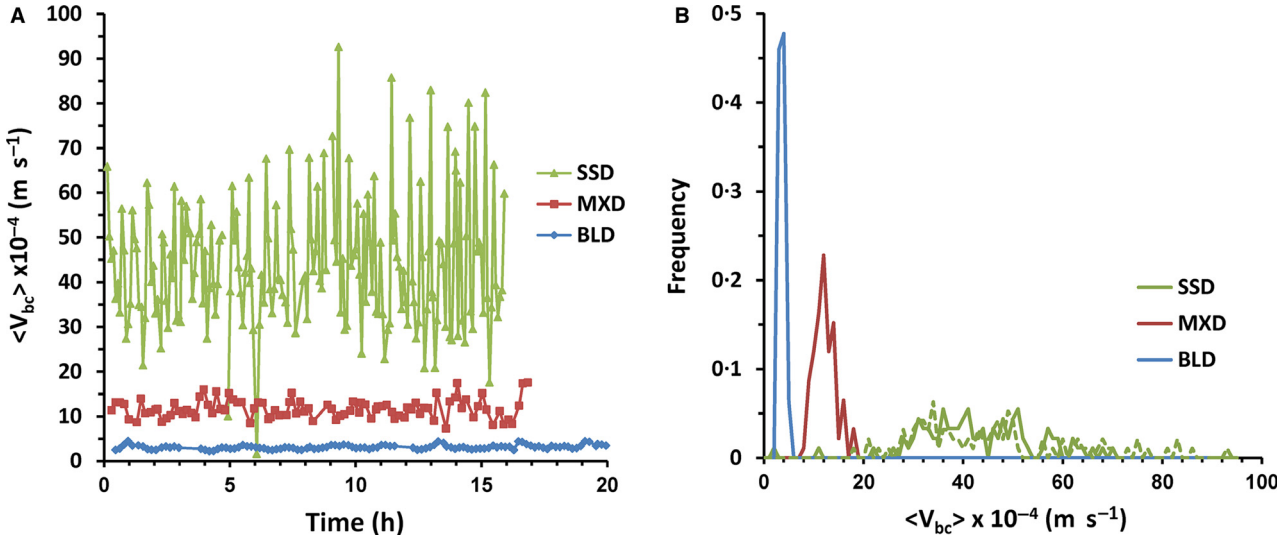

Fig. 11. Time series of spatially averaged bedform (A) migration rates $<V_{bc}>$ and (B) histograms $<V_{bc}>$ for each transport stage. The solid and dashed line in panels (C) and (D) are for the first and last 8 h of the SSD run, respectively. SSD, suspended-load dominated conditions; MXD, mixed-load dominated conditions; BLD, bedload dominated conditions.

1987; Ten Brinke *et al.*, 1999; Venditti *et al.*, 2005). Calculation of β_b for a subset of the data indicated that the 0·56 value is a suitable approximation.

Table 3 summarizes the mean translation fluxes calculated using: (i) H_m and V_{bm} ($\overline{q_{T-m}}$); (ii) H_c and V_{bc} along the channel centreline ($\overline{q_{T-a}}$); and (iii) $<H_c>$ and $<V_{bc}>$ ($<\overline{q_{T-a}}>$). Because there are no V_{bm} values for the SSD run, V_{bc} measured along the channel centreline was substituted for that run. Regardless of how the values are calculated, the translation-related flux increased with transport stage. The values of $\overline{q_{T-m}}$ and $\overline{q_{T-a}}$, which should be the most closely related sediment fluxes because they are both measured along the channel centreline, are within *ca* 10% of one another suggesting that the automated method provides estimates of q_T that are similar to the dune tracking method of Simons *et al.* (1965). The value of $\overline{q_{T-a}}$ is larger than $\langle q_{T-a} \rangle$ for all runs which may be reasonably expected since the latter is a spatial average that includes bedforms that may be slowed due to interactions with the sidewalls. The coefficient of variation for the different q_T values mirrors that for V_b and H, increasing with transport stage, and are smaller for the spatial averages than along the channel centreline.

Bedform deformation flux rates

McElroy & Mohrig (2009) calculate the deformation rate from two detrended alongstream topographic profiles of bedform topography obtained at separate times. The two topographic profiles are lagged by the translation distance and the average of elevation changes that are independent of translation are summed over the bed profile as:

$$D_b = \frac{\Delta x_\eta}{2n} \sum_x |\Pi(x)| \tag{12}$$

where $\Pi(x)$ is the at-a-point elevation difference between the translated topography divided by the time between the profiles, Δx_n is the length of the translated topographic profiles and n is the number of points in a profile. As such, D_b is simply mean volume change in topography along the translated topographic profiles. McElroy & Mohrig (2009) further propose that the deformation flux can be calculated by scaling D_b to a horizontal flux using:

$$q_D = (1 - p) D_b \frac{u_s}{w_s} \tag{13}$$

where u_s is the horizontal sediment velocity and w_s is the sediment fall velocity. The ratio u_s/w_s is the ratio of the distances that a grain travels in each direction during its trajectory.

Application of the McElroy & Mohrig method is difficult for the current data set. Equation 13 uses streamwise transects through the bedform field and assumes that the sediment involved in deformation has a trajectory through the

© 2015 The Authors. Sedimentology © 2015 International Association of Sedimentologists, *Sedimentology*

water column. The bedforms in the present experiment were highly 3D and some apparent deformation occurred due to lateral fluxes and changes in bedform spacing, in many cases without suspension. The sediment involved in deformation of the bedforms had much smaller trajectories than would be predicted with Eq. 13, which can lead to overprediction of deformation flux. Furthermore, deformation flux should be calculated over the same time scale as the translation flux (Ganti *et al.*, 2013), which is integrated over a dune length (Simons *et al.*, 1965). The most appropriate time scale is the time required for a bedform to migrate one wavelength (*ca* 48 min for BLD, *ca* 17 min for MXD and *ca* 7·5 min for SSD). The 3D bedforms in the present experiments rapidly evolved as they migrated so that, by the time a bedform migrated one wavelength, they bore no resemblance to the original bedform. As a result, it is difficult to know which two bedforms to match to calculate deformation flux from transects through the bedform field at the translation time scale. Calculations of deformation are further complicated by the level of small-scale variability in the high resolution dune profiles caused by superimposed bedforms and spurs, laterally migrating lobes and saddles, and other sources of small-scale variability. These sources of deformation all have different time scales. How to remove these smaller scale sources of variability and retain the deformation signal of the major bedforms is not clear. Simply filtering this information out or removing the central part of a probability distribution to eliminate small-scale variability is arbitrary. One way to ameliorate the latter two difficulties (rapid 3D evolution and small-scale variability) is to calculate deformation rate of individual bedforms following Ganti *et al.* (2013). The problem with this approach is that it is not clear how to turn this individual bedform deformation rate into a sediment flux and the method is impractical for producing a time series of data.

As an alternative to Eq. 13, the present authors approximate the deformation flux as:

$$q_D = q_s - q_T \tag{14}$$

This limits the authors to examination of the mean fluxes for each experiment. By calculating q_D using Eq. 14, it is assumed that all bed material sediment flux not associated with bedform translation is the result of changes in the bedforms and aggradation or degradation of the bed. Sediment was recirculated in the experiments, water surface slopes were parallel to the bed surface and the observations were made under equilibrium conditions. Therefore, aggradation or degradation of the mean bed elevation should be negligible and Eq. 14 should provide a reasonable approximation of deformation flux in the bedform field. Calculated in this way, q_D increases with transport stage (Table 3); but relative to translation, it decreases from the BLD transport stage to the MXD stage, then increases from the MXD to the SSD stage.

DISCUSSION

How do bedform dimensions change with transport stage?

It is conventional in sedimentology to assume that equilibrium bedform dimensions scale with flow depth ($H = h/6$ and $L = 5\ h$) (cf. Bridge, 2003), yet there is little empirical evidence to support a specific scaling ratio between H, L and h (Allen, 1982; Venditti, 2013). Bedforms in the present experiments were larger than the expected scaling ratios for all runs (Table 4). There is more evidence in the literature that bedform geometry scales with transport stage. Yalin and collaborators (Yalin, 1972; Yalin & Karahan, 1979a) showed that bedform aspect ratios change with transport stage, increasing from BLD conditions to MXD conditions, then decreasing for SSD conditions. Data compiled by van Rijn (1984, 1993) and Lin & Venditti (2013) support this trend, as do the present observations (Fig. 12A).

The data show that the changes in bedform aspect ratio with increasing transport stage, documented in previous work (Yalin, 1972; Yalin & Karahan, 1979a; Lin & Venditti, 2013), are a reflection of the changes in H (Fig. 12B) against continuously increasing L (Fig. 12C). This suggests that bedforms should grow with transport stage until they reach their maximum H, at which point H declines with transport stage. As H approaches zero under suspended dominated conditions, effectively washing out, L increases until they disappear. However, 'low-amplitude bedwaves' on upper stage plane beds (Bennett *et al.*, 1998) suggest that some residual topography may remain.

The observed increase in the variability of H, L and H/L with transport stage implies that a

© 2015 The Authors. Sedimentology © 2015 International Association of Sedimentologists, *Sedimentology*

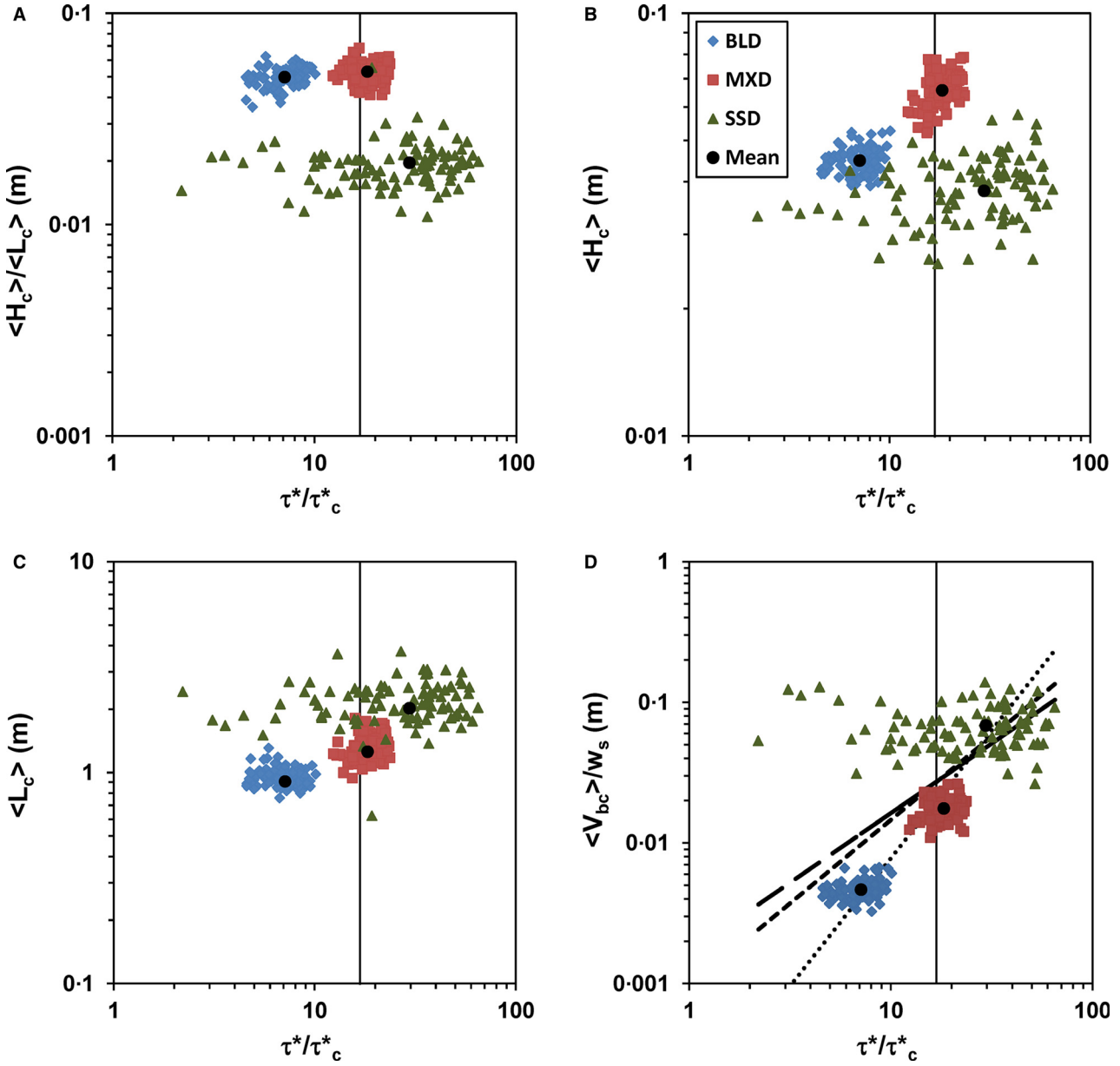

Fig. 12. Bedform (A) aspect ratio $\langle H_c \rangle / \langle L_c \rangle$, height $\langle H_c \rangle$, (C) length $\langle L_c \rangle$ and (D) dimensionless translation rate $\langle V_{bc} \rangle / w_s$ versus transport stage τ_* / τ_{*c}. The dashed line in (A) is from Yalin (1972). The long dashed line in (D) is Eq. 12 from Lin & Venditti (2013). The short dashed line and dotted lines in (D) are least-squares regression through the scatter and mean values, respectively. The solid vertical line indicates the suspension threshold. BLD, bedload dominated conditions; MXD, mixed-load dominated conditions; SSD, suspended-load dominated conditions.

wider distribution of bedform sizes and less uniform bedform fields at higher transport stage would be expected. The bed topography maps (Figs 5, 7 and 8) appear to support this idea, as do the distributions of H and L (Fig. 9C and D). Furthermore, there is an intimate linkage between the variability in the flow conditions and bedform dimensions. This link suggests that as transport stage increases, greater care is needed to ensure that measurements of bedforms are indeed representative samples of the full distribution of features on the bed.

How does bedform translation change with transport stage?

Lin & Venditti (2013) proposed an empirical model of bedform migration in rivers that

© 2015 The Authors. Sedimentology © 2015 International Association of Sedimentologists, *Sedimentology*

showed translation rate increasing with transport stage. These authors showed that grain size exerted a strong control on dune migration rates. Bedforms formed in coarser sediment move faster than in finer sediment at the same transport stage. Lin & Venditti (2013) reasoned that this is because it is more difficult to move coarser particles into suspension and normalized the bedform translation rate by the particle settling velocity (w_s) yielding the following relation:

$$\frac{V_b}{w_s} = 0.00127\left(\frac{\tau_*}{\tau_{*c}}\right)^{0.989} \times BCF \qquad (15)$$

where BCF = 1·316 and is a bias correction factor required when a log transformed variable is retransformed back into its original units.

The results support the general form of the power law relation between V_b/w_s and transport stage. A line fit through all bed surveys matches the Lin & Venditti (2013) relation with a slope of 1·19; however, a line fit to the mean values is much steeper (1·8; Fig. 12D). Nevertheless, the observed mean bedform translation rates fall within the scatter of the data used to derive the relation reported in Lin & Venditti (2013), although the BLD and MXD runs lie towards the lower end of the scatter for a given transport stage and grain size. This result might be reasonably expected because the translation rates reported here are spatially averaged across the channel and most of the data used to derive the Lin & Venditti (2013) relation were obtained by tracking individual dunes.

As with the bedform geometry, the level of variability in the migration rate increased with transport stage. Under BLD conditions, most of the bedform change between surveys occurred in the lee of the bedforms with some cross-channel change, suggesting orderly downstream bedform translation with a minor cross-stream translation. At the MXD stage, orderly downstream bedform translation still occurs, but there is a wider range of bed elevation change between surveys, there is greater cross-stream translation and greater bedform merging and splitting. At the SSD transport stage, downstream translation still occurs, but the bed evolves rapidly, cycling through different types of bedform morphology (small dunes, flat bed and large dunes). The level of variability in the data cloud for the SSD run is so large that defining a single migration rate is only possible by examining the central tendencies of data. The high level of variability at high transport stage may explain the wide scatter in the data from the literature (Lin & Venditti, 2013). The results suggest that observations of bedform migration rates based on tracking a small population of bedforms or a single bedform in a larger bedform field should be regarded with caution, which is especially the case at SSD transport stages where observed migration rates vary by two orders of magnitude at constant flow in the experiments.

What is the relation between bedform translation, deformation and the dominant transport modes?

McElroy & Mohrig (2009) reasoned that translation-related sediment flux should be equivalent to the bedload flux and that the deformation-related sediment flux should be equivalent to the suspended-sediment flux in a channel because deformation is defined as a vertical flux. The total sediment flux rate, q_T and q_D all increased with transport stage in the experiments, exhibiting power law behaviour (Fig. 13A), although the specific functional form of these relations is difficult to ascertain with only three data points.

The data do not show $q_{bl} = q_T$ or $q_{ss} = q_D$ (Table 3), but it might be overly ambitious to expect such a relation, given the inherent difficulties in accurately sampling bedload transport and the *ad hoc* method for calculating deformation flux. Nevertheless, the pattern in the ratios of bedload to translation flux and deformation to suspended-load flux are sensible. In the BLD run $q_T \approx 0{\cdot}5\ q_{bl}$, q_T increased to *ca* 2 q_{bl} in the MXD run, then declined to ca 0·9 q_{bl} at the SSD transport stage (Table 3). The increase at the MXD transport stage is noteworthy, because it suggests that suspension plays an important role in the downstream translation of bedforms in rivers, as has been previously suggested (Mohrig & Smith, 1996; Kostaschuk *et al.*, 2009). The ratio of deformation-related flux to q_{ss} at the BLD transport stage was infinity (there is no suspended-sediment flux). q_D was 0·61 q_{ss} in the MXD run and 1·15 q_{ss} in the SSD run (Table 3). While the results do not directly support the contention of McElroy & Mohrig (2009) that $q_{bl} = q_T$ or $q_{ss} = q_D$, the results are consistent with the idea that deformation and suspended load are intimately linked.

The suggestion by McElroy & Mohrig (2009) that deformation should be equivalent to the

© 2015 The Authors. Sedimentology © 2015 International Association of Sedimentologists, *Sedimentology*

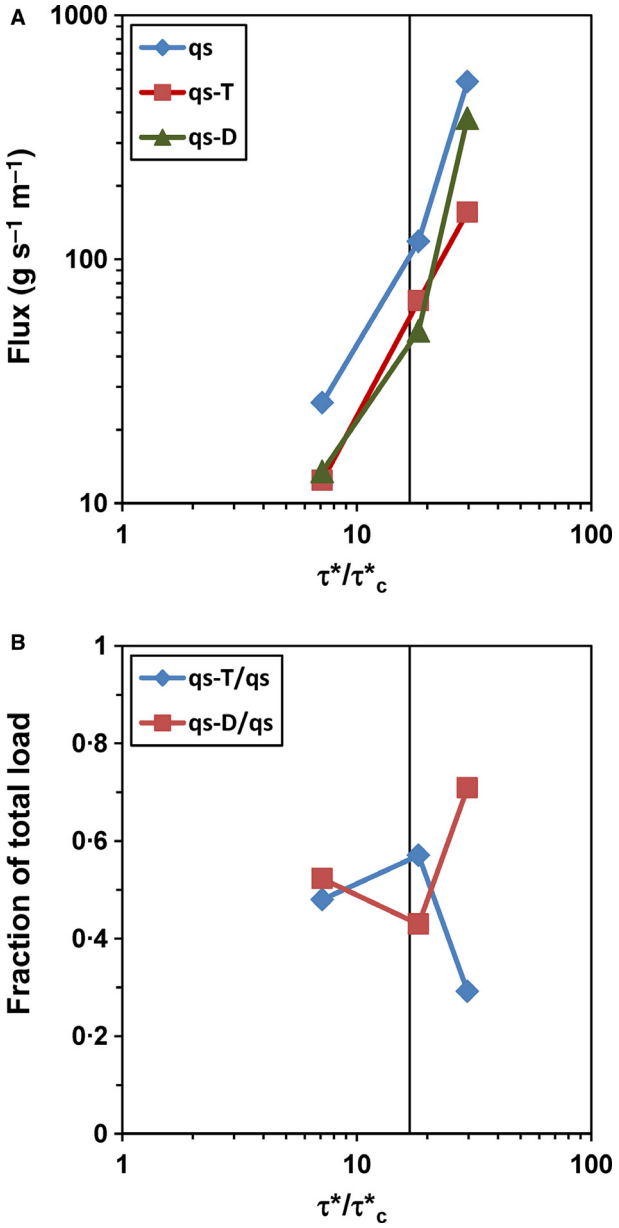

Fig. 13. (A) Change in the total (q_S), translation-related (q_T) and deformation (q_D) flux rates with transport stage. (B) The fraction of the total load contributed by q_T and q_D. The solid vertical line indicates the suspension threshold.

suspended-sediment flux is predicated on the idea that there is a vertical exchange of sediment between the bedform and the flow. However, these authors also noted that changes in shape, size and spacing of the bedforms contributed to deformation flux; these need not be associated with sediment suspension. In the present experiments, there are substantial changes in the bedform shape, size and spacing that are caused by cross-stream transport of sediment due to the 3D nature of the bedforms. This lateral translation is obvious in Fig. 7, where elevation changes are not uniform across the channel. It is likely that cross-stream transport is an important component of non-translational flux that needs to be accounted for in assessing deformation flux.

As a fraction of the total sediment flux, q_T and q_D contributed equally to the q_s at the BLD transport stage (Fig. 13B). However, as the transport stage increased, the fraction of q_s contributed by translation increased from BLD to MXD and the fraction of q_s contributed by deformation went down (Fig. 13B). This result is surprising, because it would be expected that deformation rate should increase as sediment is suspended. However, the translation rates also increased as the bedforms got bigger and the bedforms moved faster in the MXD run (Fig. 12). At the SSD transport stage, the opposite occurred: deformation flux increased and the translation flux decreased as a fraction of q_s. In the limit, it would be expected that q_D/q_s would approach one and that q_T/q_s would approach zero as the bedforms washout to a plane bed, which is consistent with the patterns in Fig. 13B.

CONCLUSIONS

1 The typical relation between bedform aspect ratio and transport stage (increasing then decreasing as more sediment is moved into suspension) is a reflection of changes in the bedform height against a background of continuously increasing bedform length. In the limit of washed-out dunes, heights approach zero and lengths approach infinity.

2 As transport stage increases, the distribution of bedform heights and lengths broadens and the features become less uniform. This suggests that, as transport stage increases, greater care is needed to ensure that measurements of bedforms are indeed representative samples of the full distribution of features on the bed.

3 Bedform translation rates generally conform to the power law relations proposed by Lin & Venditti (2013).

4 As with bedform dimensions, the distribution of bedform translation rates became broader with transport stage, to the point where translation rates can only be partly characterized by a measure of central tendency.

© 2015 The Authors. Sedimentology © 2015 International Association of Sedimentologists, *Sedimentology*

5 As a fraction of the total sediment flux, translation-related and deformation-related fluxes are approximately equivalent under bedload dominated conditions. As transport stage increases, the fraction of the flux attributed to translation increases and the fraction attributed to deformation declines. However, as the bedforms begin to washout, the opposite happens. In the limit, the fraction of the total load associated with translation approaches zero and the fraction associated with deformation approaches one, confirming the close association between deformation and suspended-sediment flux suggested by McElroy & Mohrig (2009).

ACKNOWLEDGEMENTS

This work was supported by an NSERC Discovery Grant to JV. Robert Humphries and Natalia Domarad helped undertake the experiments. We would like to thank Brandon McElroy for providing MATLAB® codes for automated calculation of bedform heights and lengths. Constructive reviews by David Mohrig, Vamsi Ganti and an anonymous reviewer greatly improved the manuscript. ML and JV designed the experiments; ML conducted the experiments and processed the data with assistance from MK. JV wrote the paper and did the data analysis presented herein.

NOTATION

a	Reference elevation above the bed in Rouse equation
C	Concentration of suspended-sediment at height z above the sediment bed
C_a	A reference concentration measured at bed elevation a in Rouse equation
$\overline{C}$	Depth averaged concentration
D	Grain size
$D_{10\ °C}$	10°C-equivalent grain size
D_{50}	Median grain size
D_b	Mean volume change in topography along translated topographic profiles
g	Gravitational acceleration
h	Flow depth
H	Bedform height
H_m	Manually measured bedform length
H_c, $<H_c>$	Characteristic bedform height and its spatial average
H_{sat}	Saturation height
l	Bed profile length
L	Bedform length
L_c, $<L_c>$	Characteristic bedform length and its spatial average
L_m	Manually measured bedform height
L_{sat}	Saturation length
n	Number of bed profile elevations
q_{ss}	Suspended-sediment flux
q_{bl}	Bedload sediment flux
q_s	Sum of q_{bl} and q_{ss}
q_T, q_{T-m}, q_{T-a}	Translation-related sediment flux, computed with H_m and V_{bm}, computed with $<H_c>$ and $<V_{bc}>$
q_D	Deformation-related sediment flux
S	Water surface slope
t	Time
u_*	Shear velocity
$U_{10\ °C}$	10°C-equivalent mean velocity
$\overline{U}$	Mean velocity
u_s	Horizontal sediment velocity
V_b	Bedform translation rate
V_{bm}	Bedform translation rate from manual method
V_{bc}, $<V_{bc}>$	Bedform translation rate from automated method and its spatial average
w	Channel width
w_s	Settling velocity of sediment
$W(l)$	Elevation variance of bed profile length l
x	Distance downstream
z	Elevation above the bed
β_b	Bedform shape factor
β	Coefficient in Rouse equation that describes the difference in sediment and fluid diffusivity
δ_b	Rate of vertical bed profile elevation change
η	Bed elevation
κ	Von Karman constant
$\Pi(x)$	Rate of 'at a point' elevation difference between the translated topography profiles
ρ_s and ρ_w	Sediment and water densities
τ_0	Shear stress from depth-slope product
τ	Wall corrected shear stress
τ_*, τ_{*c}	Shields number and its critical value for sediment entrainment
τ_*/τ_{*c}	Transport stage
Δx_n	Length of translated topographic profiles

REFERENCES

Allen, J.R.L. (1970) A quantitative model of climbing ripples and their cross-laminated deposits. *Sedimentology*, **14**, 5–26.

Allen, J.R.L. (1973) Features of cross-stratified units due to random and other changes in bed forms. *Sedimentology*, **20**, 189–202.

© 2015 The Authors. Sedimentology © 2015 International Association of Sedimentologists, *Sedimentology*

Allen, J.R.L. (1982) *Sedimentary Structures: Their Character and Physical Basis*. Elsevier, New York, NY.

Bagnold, R.A. (1966) *An Approach to the Sediment Transport Problem for General Physics*. U.S. Geol. Surv. Prof. Pap., 422-I, Geological Survey, Washington.

Bagnold, R.A. (1973) The nature of saltation and bed-load transport in water. *Proc. R. Soc. London*, **332**, 473–504.

Bennett, S.J., **Bridge, J.S.** and **Best, J.L.** (1998) Fluid and sediment dynamics of upper-stage plane beds. *J. Geophys. Res.*, **103**, 1239–1274.

Bradley, R.W., **Venditti, J.G.**, **Kostaschuk, R.A.**, **Church, M.**, **Hendershot, M.** and **Allison, M.A.** (2013) Flow and sediment suspension events over low-angle dunes: Fraser Estuary, Canada. *J. Geophys. Res.*, **118**, doi:10.1002/jgrf.20118.

Bridge, J.S. (2003) *Rivers and Floodplains*. Blackwell, Malden, MA.

Bridge, J.S. and **Tye, R.S.** (2000) Interpreting the dimension of ancient channel bars, channels, and channel belts from wireline-logs and cores. *AAPG Bull.*, **84**, 1205–1228.

Brownlie, W.R. (1981) *Prediction of Flow Depth and Sediment Discharge in Open Channels*. Report No. KH-R-43A. W. M. Keck Laboratory of Hydraulics and Water Resources, California Institute of Technology, Pasadena, CA, 232 pp.

Church, M. (2006) Bed material transport and the morphology of alluvial river channels. *Annu. Rev. Earth Planet. Sci.*, **34**, 325–354.

Coleman, S.E. and **Melville, B.W.** (1994) Bed-form development. *J. Hydraul. Eng.*, **120**, 544–560.

Dietrich, W.E. (1982) Settling velocity of natural particles. *Water Resour. Res.*, **18**, 1615–1626.

Dietrich, W.E. and **Smith, J.D.** (1984) Bed load transport in river meander. *Water Resour. Res.*, **20**, 1355–1380. doi:10.1029/WR020i010p01355.

Fredsoe, J. (1982) Shape and dimensions of stationary dunes in rivers. *J. Hydr. Div.*, **108**, 932–947.

Ganti, V., **Paola, C.** and **Foufoula-Georgiou, E.** (2013) Kinematic controls on the geometry of the preserved cross sets. *J. Geophys. Res. Earth Surf.*, **118**, 1296–1307.

Helley, E.J. and **Smith, W.** (1971) Development and calibration of a pressure-difference bedload sampler. *U.S. Geol. Surv. Open-File Rep.*, 1–18.

Jerolmack, D.J. and **Mohrig, D.** (2005) Frozen dynamics of migrating bedforms. *Geology*, **33**, 57–60.

Kostaschuk, R.A. and **Villard, P.V.** (1996) Flow and sediment transport over large subaqueous dunes: Fraser River, Canada. *Sedimentology*, **43**, 849–863.

Kostaschuk, R., **Shugar, D.**, **Best, J.**, **Parsons, D.**, **Lane, S.**, **Hardy, R.** and **Orfeo, O.** (2009) Suspended sediment transport and deposition over a dune: Río Paraná, Argentina. *Earth Surf. Proc. Land.*, **34**, 1605–1611.

Leclair, S.F. (2002) Preservation of cross-strata due to the migration of subaqueous dunes: an experimental investigation. *Sedimentology*, **49**, 1157–1180.

Lin, C.-Y.M. (2011) *Bedform Migration in Rivers*. M.Sc. Thesis, Simon Fraser University, Burnaby, British Columbia, Canada, 147 pp.

Lin, C.-Y.M. and **Venditti, J.G.** (2013) An empirical model of subcritical bedform migration. *Sedimentology*, **60**, 1786–1799.

Lopez, F. and **Garcia, M.** (2001) Risk of sediment erosion and suspension in turbulent flows. *J. Hydraul. Eng.*, **127**, 231–235.

McElroy, B.J. (2009) *Expressions and Implications of Sediment Transport Variability in Sandy Rivers*. Ph.D. dissertation, University of Texas at Austin, Austin, TX.

McElroy, B. and **Mohrig, D.** (2009) Nature of deformation of sandy bed forms. *J. Geophys. Res.*, **114**, F00A04. doi:10.1029/2008JF001220.

Miller, M.C., **McCave, I.N.** and **Komar, P.D.** (1977) Threshold of sediment motion under unindirectional currents. *Sedimentology*, **41**, 883–903.

Mohrig, D. and **Smith, J.D.** (1996) Predicting the migration rates of subaqueous dune. *Water Resour. Res.*, **32**, 3207–3217.

Nino, Y. and **Garcia, M.H.** (1998) On England's analysis of turbulent energy and suspended load. *J. Hydraul. Eng.*, **124**, 480–483.

Paola, C. and **Borgman, L.** (1991) Reconstructing random topography from preserved stratification. *Sedimentology*, **38**, 553–565.

Raudkivi, A.J. (1967) *Loose Boundary Hydraulics*. Pergamon, Oxford.

Raudkivi, A.J. and **Witte, H.H.** (1990) Development of bed features. *J. Hydraul. Eng.*, **116**, 1063–1079.

Sklar, L.S. and **Dietrich, W.E.** (2004) A mechanistic model for river incision into bedrock by saltating bed load. *Water Resour. Res.*, **40**, W06 301.

Southard, J.B. and **Boguchwal, L.A.** (1990) Bed configurations in steady unidirectional water flow part 2. Synthesis of flume data. *J. Sed. Petrol.*, **60**, 658–679.

van Rijn, L.C. (1984) Sediment transport III: bed forms and alluvial roughness. *J. Hydraul. Eng.*, **110**, 1733–1754.

van Rijn, L.C. (1993) *Principles of Sediment Transport*. Aqua, Amsterdam.

Rouse, H. (1939) Experiments on the mechanics of sediment suspension. In: *Proceedings 5th International Congress on Applied Mechanics*, pp. 550–554. Wiley, New York.

Rubin, D.M. and **Hunter, R.E.** (1982) Bedform climbing in theory and nature. *Sedimentology*, **29**, 121–138.

Simons, D.B., **Richardson, E.V.** and **Nordin, C.F.** (1965) Bedload equation for ripples and dunes. *U.S. Geol. Surv. Prof. Pap.*, **462-H**, 1–9.

Ten Brinke, W.B.M., **Wilbers, A.W.E.** and **Wesseling, C.** (1999) Dune growth, decay and migration rates during a large-magnitude flood at a sand and mixed-gravel bed in the Dutch Rhine river system. In: *Fluvial Sedimentology VI* (Eds N.D. Smith and J. Rogers), *Spec. Publ. Int. Assoc. Sedimentol.*, **28**, pp. 15–32. Blackwell Science, Malden, MA.

Van den Berg, J.H. (1987) Bedform migration and bed-load transport in some rivers and tidal environments. *Sedimentology*, **34**, 681–698.

Venditti, J.G. (2013) Bedforms in sand-bedded rivers. In: *Treatise on Geomorphology, Fluvial Geomorphology* (Eds J. Shroder Jr and E. Wohl), pp. 137–162. Academic Press, San Diego, CA.

Venditti, J.G., **Church, M.** and **Bennett, S.J.** (2005) Morphodynamics of small-scale superimposed sand waves over migrating dune bed forms. *Water Resour. Res.*, **41**, W10423. doi:10.1029/2004WR003461.

Williams, G.P. (1970) Flume width and water depth effects in sediment-transport experiments. *U.S. Geol. Surv. Prof. Pap.*, **562-H**, 1–37.

Yalin, M.S. (1972) *Mechanics of Sediment Transport*. Pergamon Press, Oxford.

Yalin, M.S. and **Karahan, E.** (1979a) Steepness of sedimentary dunes. *J. Hydraul. Div.*, **105**4, 381–392.

Yalin, M.S. and **Karahan, E.** (1979b) Inception of sediment transport. *J. Hydraul. Div.*, **105**, 1433–1443.

Manuscript received 15 October 2014; revision accepted 16 October 2015

© 2015 The Authors. Sedimentology © 2015 International Association of Sedimentologists, *Sedimentology*